SCIENTIFIC REPORTS

OPEN

Received: 11 October 2015
Accepted: 05 January 2016
Published: 04 February 2016

Hybrid magnetoresistance in Pt-based multilayers: Effect originated from strong interfacial spin-orbit coupling

Kangkang Meng[1], Jiaxing Xiao[2], Yong Wu[1], Jun Miao[1], Xiaoguang Xu[1], Jianhua Zhao[2] & Yong Jiang[1]

The hybrid magnetoresistance (MR) behaviors in Pt/$Co_{90}Fe_{10}$/Pt, $Mn_{1.5}$Ga/Pt and $Mn_{1.5}$Ga/Pt/$Co_{90}Fe_{10}$/Pt multilayers have been investigated. Both planer Hall effect (PHE) and angle-dependent MR in Pt/$Co_{90}Fe_{10}$/Pt revealed the combination of spin Hall MR (SMR) and normal anisotropic MR (AMR), indicating the large contribution of strong spin-orbit coupling (SOC) at the interfaces. When Pt contacted with perpendicular magnetic anisotropy (PMA) metal $Mn_{1.5}$Ga, the strong interfacial SOC modified the effective anomalous Hall effect. The MR in $Mn_{1.5}$Ga/Pt/$Co_{90}Fe_{10}$/Pt is not a simple combination of SMR and AMR, but ascribed to the complicated domain wall scattering and strong interfacial SOC when Pt is sandwiched by the in-plane magnetized $Co_{90}Fe_{10}$ and the PMA $Mn_{1.5}$Ga.

Magnetoresistance (MR) is the property of a material to change the value of its electrical resistance under an external magnetic field. The dependence of resistance on the angle between current and magnetization in metallic ferromagnets (FM) is called anisotropic magnetoresistance (AMR)[1]. On the other hand, planar Hall effect (PHE) and anomalous Hall effect (AHE) are both observed as a voltage transverse to the applied current in contrast to AMR, which is measured in longitudinal geometry[2–5]. The longitudinal resistivity ρ_{xx} denoting AMR and the transverse resistance ρ_{xy} characterizing PHE are given by:

$$\rho_{xx} = \rho_{\perp} + (\rho_{\parallel} - \rho_{\perp})m_x^2 \quad (1)$$

$$\rho_{xy} = (\rho_{\parallel} - \rho_{\perp})m_x m_y \quad (2)$$

where $\rho_{\parallel}$ ($\rho_{\perp}$) is the resistivity along (perpendicular to) the direction of the in-plane component of magnetization (**M**), m_x, m_y are the components of the in-plane magnetization along *x* and *y* directions respectively. For the ordinary AMR effect in magnetic layers, ρ_{xx} only depends on the magnetization component parallel to current.

Recently, a new type of MR is observed when a strong spin-orbit coupling (SOC) metal such as Pt comes in contact with a FM, either metallic or insulating[6–15]. In these hybrid structures, spin and charge transport phenomena are interconnected, and Pt may serve as both spin current generator and detector[12–16]. The spin Hall effect (SHE) can convert charge current into pure spin current in the transverse direction and the conversion is enhanced in heavy metals such as Pt due to their strong SOC. The spin current can be used to apply torque to magnetic moment by direct transfer of spin angular momentum[17–20]. On the other hand, it can also be detected by inverse spin Hall effect (ISHE), which converts the pure spin current into charge current resulting in charge accumulation along the transverse direction. Nakayama *et al.* had presented the unusual MR of Pt/ yttrium iron garnet (YIG) in terms of a nonequilibrium proximity effect caused by the simultaneous action of SHE and ISHE and therefore called it spin Hall MR (SMR)[12]. The experiments were theoretically explained by Chen *et al.* who proposed a SMR theory based on the spin-diffusion approximation in a Pt layer in the presence of spin-orbit interaction and quantum mechanical boundary conditions at the Pt/YIG interface in terms of spin-mixing

[1]School of Materials Science and Engineering, University of Science and Technology Beijing, Beijing 100083, China. [2]State Key Laboratory of Superlattices and Microstructures, Institute of Semiconductors, Chinese Academy of Sciences, Beijing 100083, China. Correspondence and requests for materials should be addressed to K.K.M. (email: kkmeng@ustb.edu.cn) orY.J. (email: yjiang@ustb.edu.cn)

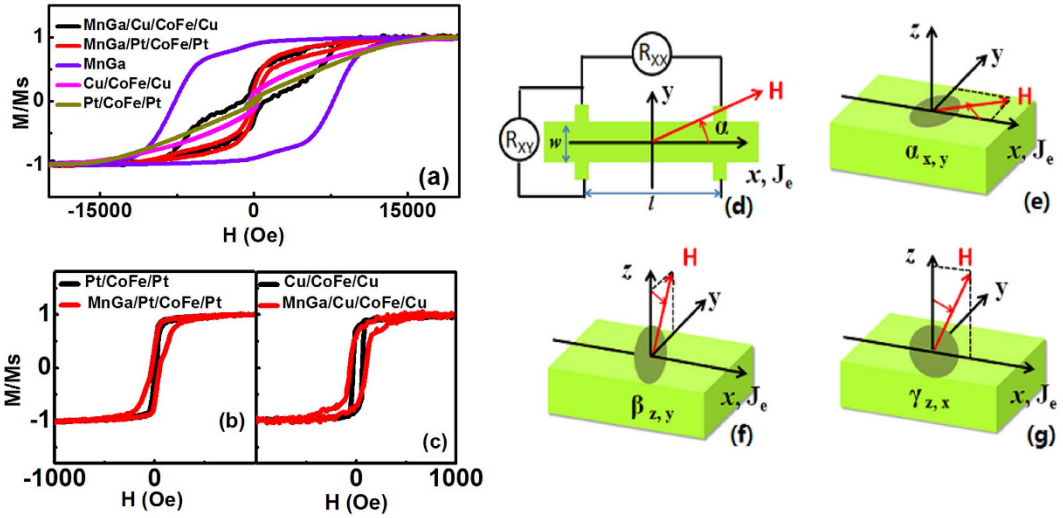

Figure 1. Magnetic properties. (**a–c**) The normalized out-of-plane and in-plane magnetic hysteresis loops at 300 K. (**d**) Schematic diagram of the longitudinal (R_{XX}) and transverse (R_{XY}) resistance measurements. The charge current $\mathbf{J_e}$ is along ***x*** axis. (**e–g**) Schematic diagram of the magnetic field applied in ***xy, zy,*** and ***zx*** planes with angles α_{xy}, β_{zy} and γ_{zx}, respectively.

conductance[13]. At the interface the electrons in Pt will interact with the localized moment in the FM. A part of spin current is absorbed by the magnetization as spin-transfer torque and the spin-current reflection is thus suppressed. This absorption is zero when the magnetization **M** is parallel to the spin-current polarization **σ** and maximized when **M** is perpendicular to **σ**. By changing the magnetization direction of the FM, the polarization direction of the reflected spins and thus the direction of the additional created charge current can be controlled, and a transverse voltage is also generated. In a word, the SMR is a strong interfacial SOC phenomenon.

However, the reports of SMR, so far, have mostly focused on Pt/YIG bilayers, because one can easily access the magnetotransport properties of the Pt thin film deposited on the insulating FM YIG. There is a challenge to detect the mechanism of the strong interfacial SOC when Pt contacts with a normal FM such as CoFe. Meanwhile, how about the phenomena when Pt contacts with perpendicular magnetic anisotropy (PMA) metals since SMR is also influenced by perpendicular magnetization component? In the past two decades, PMA Mn_xGa ($1 < x < 1.8$) alloy thin films with $L1_0$ structure have gained increasing attention for possible application in ultrahigh density magnetic recording media, permanent magnets and spintronics[21,22]. Therefore, there is also a fundamental interest to explore the spin current related phenomena when Pt contacts with a PMA Mn_xGa.

In this work, we have investigated MR behaviors in Pt/$Co_{90}Fe_{10}$/Pt, $Mn_{1.5}Ga$/Pt and $Mn_{1.5}Ga$/Pt/$Co_{90}Fe_{10}$/Pt multilayers ($Co_{90}Fe_{10}$ and $Mn_{1.5}Ga$ will be simply noted as CoFe and MnGa in the following paragraph), in which CoFe is polycrystalline and MnGa is a single-crystalline PMA metal. The magnetic and transport properties are compared with the multilayers in which Pt is replaced by Cu with a weak SOC. The PHE of Pt/CoFe/Pt is much larger than that of Cu/CoFe/Cu. On the other hand, as compared with normal AMR in Cu/CoFe/Cu, the angle-dependent MR in Pt/CoFe/Pt reveals that the longitudinal resistivity change is also related with the magnetization perpendicular to the current direction in the film plane. The phenomenon indicates a large contribution of strong SOC at the interface. When Pt contacts with PMA MnGa, the effective AHE becomes smaller, which also confirms the strong interfacial scattering due to SOC. The MR in MnGa/Pt/CoFe/Pt is not a simple combination of SMR and AMR but ascribed to the complicated domain wall scattering and SOC when Pt is sandwiched by the in-plane CoFe and the PMA MnGa.

Results

Magnetic properties. The out-of-plane and in-plane hysteresis loops of all the fabricated multilayers and a single 20-nm-thick MnGa film are shown in Fig. 1a–c. The perpendicular **M-H** curve of MnGa shows a square-like shape revealing its giant PMA. Although Pt/CoFe/Pt and Cu/CoFe/Cu exhibit similar magnetization reversal in perpendicular component, the M-H curves of MnGa/Pt/CoFe/Pt and MnGa/Cu/CoFe/Cu show different domain structures. Both Pt/CoFe/Pt and Cu/CoFe/Cu show typical in-plane magnetic anisotropy and have almost the same saturated magnetization. However their coercivities are different, indicating delicately different micromagnetic configurations of domain walls. Both coercivities and saturation fields of MnGa/Cu/CoFe/Cu and MnGa/Pt/CoFe/Pt have been enhanced and their values are almost the same as shown in the curves parallel to the plane in Fig. 1b,c.

All the samples were fabricated into Hall bars with a nominal length *l* of 2.5 mm and a width *w* of 0.2 mm. Figure 1d shows the resistance measurement geometry of the Hall bars in the ***xy*** plane with a current along ***x*** and the configurations for longitudinal R_{XX} and transverse resistance R_{XY}. For subsequent measurements, the magnetic field was applied in the ***xy, zy,*** and ***zx*** planes with angles α_{xy}, β_{zy} and γ_{zx} (simply noted as α, β and γ) respectively, as shown in Fig. 1e–g.

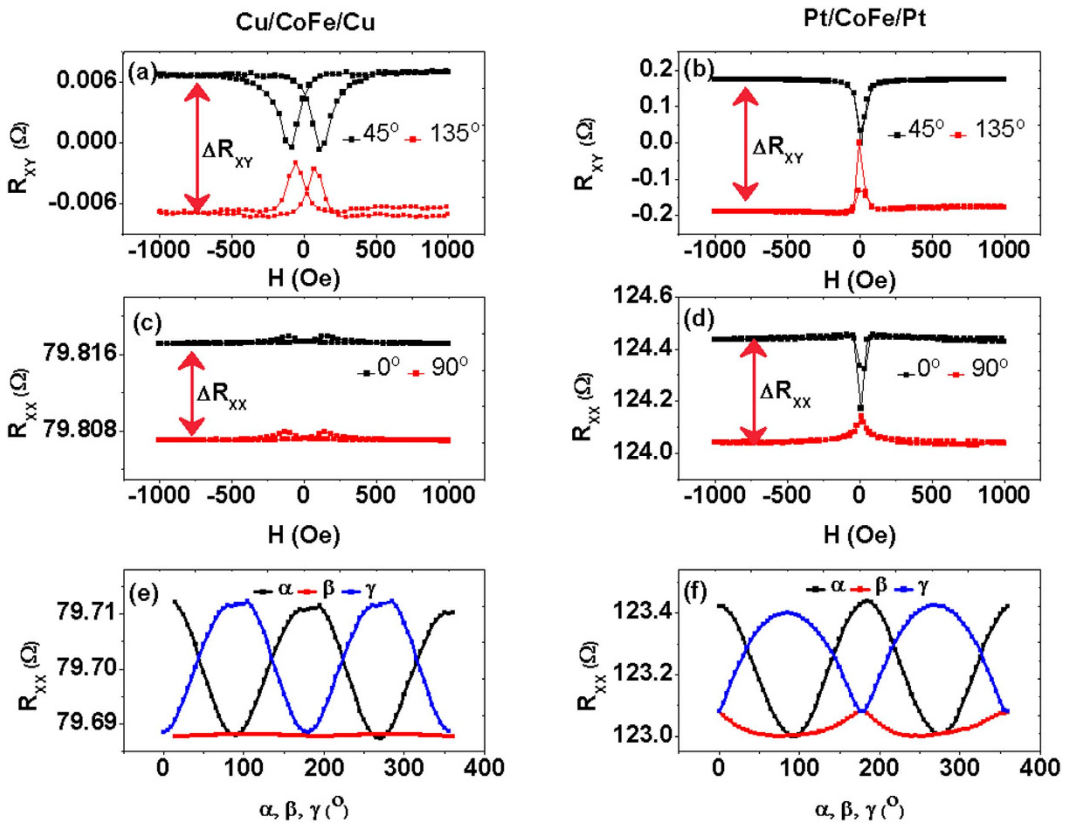

Figure 2. PHE and MR of Cu/CoFe/Cu and Pt/CoFe/Pt. (**a,b**) Measurements of R_{XY} in Cu/CoFe/Cu and Pt/CoFe/Pt with the applied magnetic field forming a fixed angle ($\alpha = 45°$ and $\alpha = 135°$) with the current. (**c,d**) Measurements of R_{XX} with the applied magnetic field forming a fixed angle ($\alpha = 0°$ and $\alpha = 90°$) with the current. (**e,f**) The α, β and γ dependence of R_{XX} with a magnetic field of 6 T.

Hybrid MR in Pt/CoFe/Pt. The AMR (R_{XX}) and PHE (R_{XY}) measured at low magnetic field ($\mathbf{H} = 1000$ Oe) and the angle-dependent MR measured at high field ($\mathbf{H} = 6$ T) of Pt/CoFe/Pt and Cu/CoFe/Cu are shown in Fig. 2. In Fig. 2a,b, the measurements of PHE were done with the applied magnetic field forming a fixed angle ($\alpha = 45°$ and 135°) with the current, since the signal will be maximized in this geometry as shown in equation (2). After subtracting the common offset, the signals with opposite sign were obtained. On the other hand, the AMR measurements with maximized signals were done with the applied field keeping a fixed angle with the current ($\alpha = 0°$ and 90°) shown in Fig. 2c,d. It is observed that both the resistance change ΔR_{XX} and ΔR_{XY} of Pt/CoFe/Pt are all much larger than those of Cu/CoFe/Cu. Considering the thickness and polycrystalline structure of the CoFe layer, the MR caused by magnetic domain walls for the two multilayers should all be quite small. The enhancement of the resistance change in Pt/CoFe/Pt may mostly be contributed by SMR. The longitudinal and transverse resistivity change for SMR can be formulated as[13]:

$$\rho_{xx} \approx \rho + \Delta\rho_0 + \Delta\rho_1\left(1 - m_y^2\right) \tag{3}$$

$$\rho_{xy} \approx \Delta\rho_1 m_x m_y + \Delta\rho_2 m_z \tag{4}$$

where ρ is the intrinsic electric resistivity, $\Delta\rho_0$ is the resistivity reduced by the spin-orbit interaction, m_z is the component of the magnetization in $\boldsymbol{z}$ direction. $\Delta\rho_1$ and $\Delta\rho_2$ are the magnitude of the resistivity related to the complex spin-mixing interface conductance $G_{\uparrow\downarrow} = G_r + iG_i$. $\Delta\rho_1$ (caused mainly by G_r) contributes to the conductance modulation depending on the in-plane component of the magnetization, while $\Delta\rho_2$ (caused mainly by G_i) contributes only when there is a magnetization component normal to the plane. Therefore, the resistance change not only depends on m_x in ordinary AMR but also on m_y in SMR. Meanwhile, for both longitudinal and transverse configurations, there are peaks or dips observed around the coercivity, and they also depend on the field direction. It is proposed that the magnetization of CoFe will be fully rotated in-plane towards **H** due to its in-plane magnetic anisotropy. This magnetic rotation results in a change in measured resistance, passing the maximum or minimum resistance, which is observed as a peak or dip around the coercivity. Figure 2e,f show the α, β and γ dependence of R_{XX} in Pt/CoFe/Pt and Cu/CoFe/Cu respectively. Cu/CoFe/Cu exhibits a normal AMR of a polycrystalline ferromagnetic film with in-plane anisotropy: $R_{XXL} > R_{XXT}$, $R_{XXT} \approx R_{XX\perp}$[1], where R_{XXL}, R_{XXT} and $R_{XX\perp}$ are longitudinal resistances when $\alpha = 0°$, $\alpha = 90°$ and $\beta = 0°$ respectively. For Pt/CoFe/Pt, $R_{XX}(\alpha)$ shows the $\cos^2\alpha$ dependence but have a feature of $R_{XXL} > R_{XX\perp} > R_{XXT}$, which is different from pure AMR or SMR

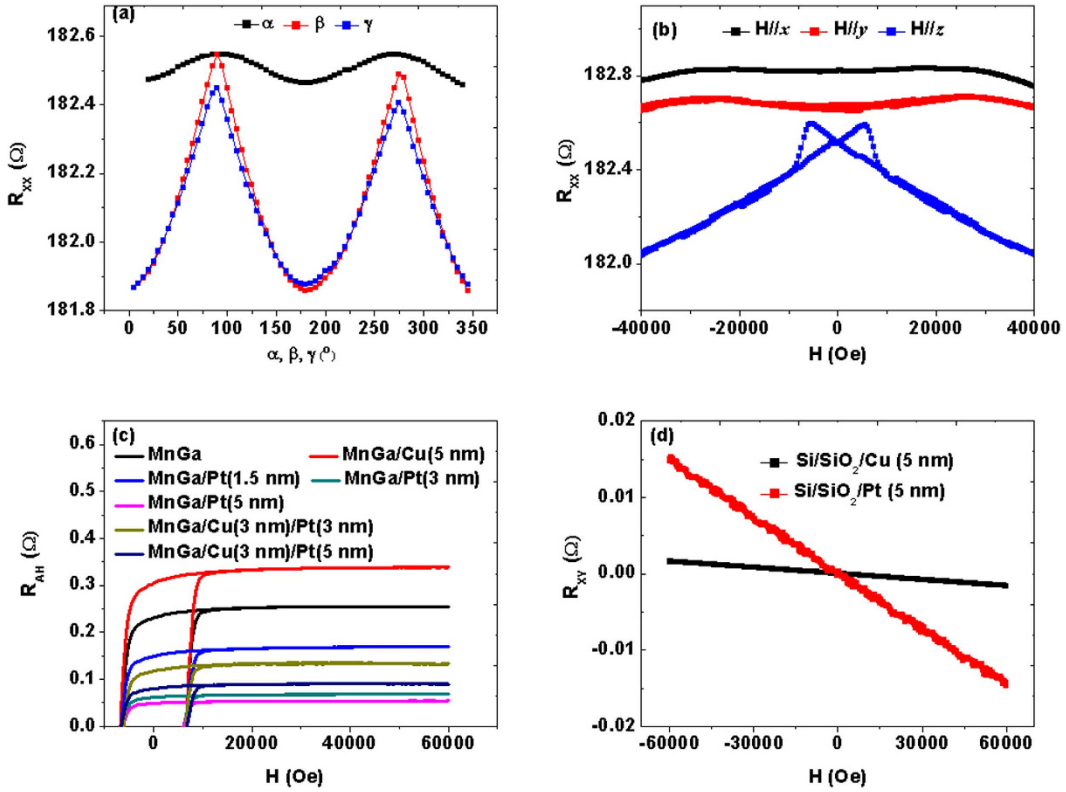

Figure 3. Magnetotransport properties of MnGa, MnGa/Cu and MnGa/Pt. (**a**) The α, β and γ dependence of R_{XX} for MnGa with a magnetic field of 6 T. (**b**) The field dependent R_{XX} with **H** along the ***x, y,*** and ***z*** directions respectively. (**c**) Anomalous Hall effect of MnGa, MnGa/Cu(5), MnGa/Pt(*t*) ($t = 1.5 \sim 5$ nm), MnGa/Cu(3)/Pt(3) and MnGa/Cu(3)/Pt(5). (**d**) Hall effect of the 5-nm-thick Pt and Cu layers grown on Si/SiO_2 substrates.

because the γ scan of R_{XX} does not keep constant[12]. $R_{XX}(\beta)$ shows the $-\sin^2\alpha$ dependence, which is consistent with equation (3). Furthermore, the SMR ($\Delta\rho_1/\rho$) can be formulated as[13]

$$\frac{\Delta\rho_1}{\rho} = \theta_{SH}^2 \frac{\lambda}{d_N} \mathrm{Re} \frac{2\lambda G_{\uparrow\downarrow} \tanh^2 \frac{d_N}{2\lambda}}{\sigma + 2\lambda G_{\uparrow\downarrow} \coth \frac{d_N}{\lambda}}, \quad (5)$$

where θ_{SH} is the spin hall angle, d_N the thickness of heavy metal layer, $\sigma = \rho^{-1}$ the conductivity and λ the spin diffusion length. By fitting the angular dependence curves in Fig. 2f, we firstly obtain $\Delta\rho_1 = 6.4 \times 10^{-3}\,\mu\Omega$cm and SMR $= \Delta\rho_1/\rho \approx 0.06\%$. Using the parameters $\theta_{SH} = 0.05$ and $\lambda = 1.5$ nm for Pt[13], the spin mixing conductance $G_{\uparrow\downarrow}$ of the multilayers can be deduced from Eq. (5) as about $2.6 \times 10^{10}\,\Omega^{-1}\mathrm{m}^{-2}$. All the results reveal the combination of SMR and normal AMR, indicating the large contribution of strong SOC at the interfaces.

Spin current related transport properties of the PMA MnGa/Pt bilayers. Firstly, we measured the transport properties of a single MnGa layer. Figure 3a shows the α, β and γ dependence of R_{XX}. R_{XX} (α) shows the $\sin^2$ (α) dependence while R_{XX} (β) and R_{XX} (γ) all adapt $\sin^4$ dependence on the angle. Figure 3b shows the field dependent resistance with **H** along the ***x, y,*** and ***z*** directions respectively. It is obviously seen from the two figures that the most dramatic resistance change happens when the magnetization is out of the plane, which is caused by the special domain structure of MnGa. Then we studied the thickness dependence of AHE resistance R_{AH} in $Mn_{1.5}Ga/Pt$ (*t*) ($t = 1 \sim 5$ nm), as compared with those of MnGa and MnGa/Cu shown in Fig. 3c. The R_{AH} was obtained by subtracting the ordinary Hall component (determined from a linear fit to the high-field region up to ±6 T). The Hall effect measurements of Pt (5 nm) and Cu (5 nm) grown on Si/SiO_2 substrates show only the ordinary Hall effect with the Hall voltage linearly dependent on **H** as shown in Fig. 3d. The ordinary Hall effect is relatively small and will not dramatically influence the Hall effect in MnGa/Cu and MnGa/Pt. From Fig. 3c we can find that the R_{AH} in MnGa/Cu (5) is larger than that in a single epitaxial MnGa film, while the R_{AH} values in all the MnGa/Pt(*t*) bilayers become smaller. After inserting Cu between MnGa and Pt, the R_{AH} in MnGa/Cu(3)/Pt(3) and MnGa/Cu(3)/Pt(5) become larger than those in the films with direct contact but a little bit smaller than that in the single MnGa film. It has been proved that Cu is very far from the Stoner instability and the nonlocal exchange force does not reach over such a thickness. Meanwhile, Cu has a long (several hundred nanometers) spin diffusion length and a very small SHE due to weak SOC, and could carry spin current over a long distance. Altering the interface by inserting Cu can block the interfacial SOC induced by Pt. Therefore, the observation of

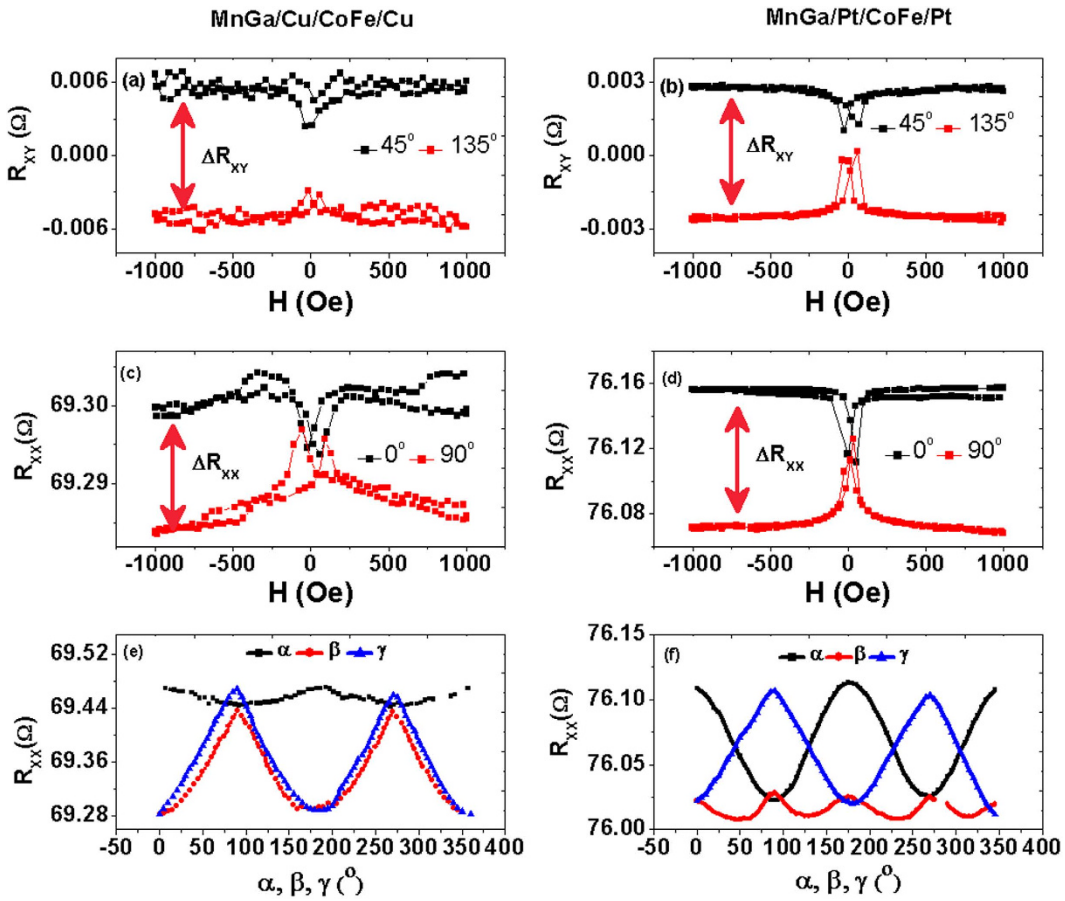

Figure 4. PHE and MR of MnGa/Cu/CoFe/Cu and MnGa/Pt/CoFe/Pt. (**a,b**) Measurements of R_{XY} in MnGa/Cu/CoFe/Cu and MnGa/Pt/CoFe/Pt with the applied magnetic field forming a fixed angle ($\alpha = 45°$ and $\alpha = 135°$) with the current. (**c,d**) Measurements of R_{XX} with the applied magnetic field forming a fixed angle ($\alpha = 0°$ and $\alpha = 90°$) with the current; (**e,f**) The α, β *and* γ dependence of R_{XX} with a magnetic field of 6 T.

the modified AHE cannot be explained by the influence of a magnetized Pt layer induced by magnetic proximity effect but mostly depend on the SHE of the heavy metals.

Magnetotransport properties in MnGa/Pt/CoFe/Pt and MnGa/Cu/CoFe/Cu. The most complicated transport properties have been observed in MnGa/Pt/CoFe/Pt, and the results of the multilayers and the reference sample MnGa/Cu/CoFe/Cu are shown in Fig. 4. Before carrying out the measurement of AMR and PHE at low field range, a high magnetic field of 6 T was firstly applied along ***z*** axis of the samples to induce perpendicular magnetization of MnGa and then decreased to zero. As compared with Cu/CoFe/Cu, both ΔR_{XX} and ΔR_{XY} of MnGa/Cu/CoFe/Cu are very small as shown in Fig. 4a,c, which are also consistent with equation (1) and (2). However, the resistance changes in MnGa/Pt/CoFe/Pt become dramatic, especially for ΔR_{XY}. The results are not consistent with the mechanism of either SMR or AMR. For the low field measurement, the strong and complex interfacial SOC have decreased PHE when Pt is sandwiched by the in-plane CoFe and PMA MnGa, but R_{XY} still shows the sin 2α dependence. On the other hand, the angle-dependent MR of MnGa/Cu/CoFe/Cu measured at high field reveals a combination of Cu/CoFe/Cu and MnGa. $R_{XX}(\alpha)$ shows the $\cos^2(\alpha)$ dependence while R_{XX} (β) and R_{XX} (γ) show similar angle dependence with those of MnGa, as shown in Fig. 4e. For MnGa/Pt/CoFe/Pt, R_{XX} (β) shows a distinctive behavior, which adapts the dependence of $\cos^2$ (2β). In this case, the magnetization is perpendicular to the current in the film plane all through the measurement, which indicates the combination of both complicated domain wall scattering and strong interfacial SOC when Pt is sandwiched between the in-plane magnetized CoFe and PMA MnGa films.

High magnetic field dependent resistance. To further study the transport properties induced by domain wall scattering, we also measured the high magnetic field dependent resistance of the four multilayers with a field **H** along the ***x***, ***y***, and ***z*** directions respectively. In Fig. 5a,b, the in-plane curves (**H**//***x*** and **H**//***y***) of both Cu/CoFe/Cu and Pt/CoFe/Pt show steep resistivity changes at small fields (<1000 Oe), but for H//z the curves indicate coherent magnetization rotation which is completed at about 1.8 T. At large fields, the films become homogeneously magnetized, all the curves exhibit linear decrease which is usually referred to as the spin-disorder MR caused by the suppression of spin waves with increasing field strength[1]. It is indicated that the difference of

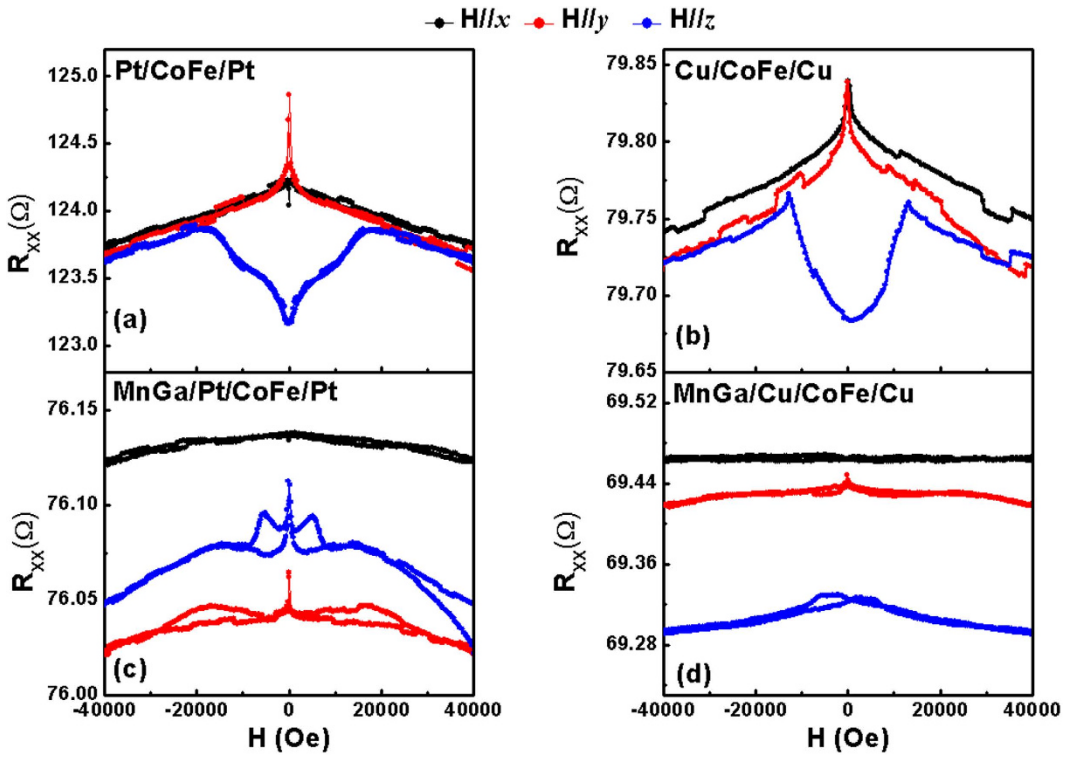

Figure 5. The high magnetic field dependent resistance R_{XX} of the four multilayers with a field H along the *x*, *y*, and *z* directions respectively.

domain wall scattering between Cu/CoFe/Cu and Pt/CoFe/Pt is not large. However, the field dependent resistance in MnGa/Pt/CoFe/Pt becomes much more complicated compared with that in MnGa/Cu/CoFe/Cu. When the current is applied along ***x*** directions, the high magnetic field dependence of R_{XX} for the two samples is almost the same. In contrast, when the magnetization is perpendicular to the current, for example **H**//***y*** and **H**//***z***, more evident resistivity changes at small fields happen. To study the resistivity due to domain wall scattering, Levy and Zhang developed a quantum mechanical description based on the giant MR Hamiltonian which leads to an increased resistance due to the mixing of the spin conduction channels induced by magnetization rotation within the domain wall[23]. Noticeably, they were the first to derive both the CIW (current in wall) and CPW (current perpendicular to wall) resistances. Viret *et al.* carried out the low-temperature measurements of the resistance induced by magnetic domain walls in FePd with perpendicular anisotropy in the CPW and CIW configurations, which quantitatively agreed with the model of Levy and Zhang[24]. They have found that the resistance variation in these two configurations are quite different, which reflects the asymmetric domain wall induced increase of resistivity. Thus we ascribe the different resistance variations between current parallel (**H**//***x***) and perpendicular to the magnetic field (**H**//***y*** and **H**//***z***) to different domain wall rotation. Therefore, both strong SOC and domain wall scattering at the interfaces largely contribute to the transport properties of MnGa/Pt/CoFe/Pt and the bottom Pt layer sandwiched by MnGa and CoFe may play a dominant role. To further improve it, we investigate the magnetic and transport properties of MnGa/Pt(1.5)/CoFe/Pt(1.5) as shown in Fig. 6. Both out-of-plane and in-plane hysteresis loops reveal the existence of magnetic coupling but indicate different micromagnetic configurations of domain walls as compared with MnGa/Pt(5)/CoFe/Pt(1.5) shown in Fig. 1a. It has been found that the variations of the transport properties in the multilayers are not evident with **H**//***x***, thus we just focus on the transport behavior when the current is perpendicular to the magnetic field. The complicated behaviors of the high magnetic field dependent resistance R_{XX} with **H**//***y*** also reveal the existence of complex domain wall scattering. However, for MnGa/Pt(1.5)/CoFe/Pt(1.5), the field dependent resistance R_{XX} shows similar behavior with that in the single MnGa film when ***H***//***z***, indicating weak contribution from magnetic coupling along the ***z*** direction. Meanwhile, the β scan of R_{XX} also shows similar behavior with that in MnGa as shown in Fig. 3a. It is proved that decreasing the thickness of the bottom Pt layer decreases not only the contribution of magnetic coupling but also that from strong SOC. However, more detailed understanding of the transport properties in this kind of multilayer with different magnetic anisotropies is still a challenge and need further study.

Current dependence of SMR. In our experiment, the current of 1 mA is applied and the current density is about 10^5 A.cm^{-2}. We have also carried out the current dependence of R_{XX} (β) and R_{XY} (H) in Pt/CoFe/Pt and MnGa/Pt/CoFe/Pt multilayers with the current of 0.1, 1 and 5 mA as shown in Fig. 7. The measurements of R_{XY} (H) were done with $\alpha = 135°$. It is found that as increasing the current, the R_{XY} in both two samples are enhanced. However, the R_{XX} (β) with high magnetic field of 6 T are almost the same with different applied current for Pt/CoFe/Pt. For MnGa/Pt/CoFe/Pt, when the current is 0.1 mA, the $R_{XX}(\beta)$ reveals a more evident contribution

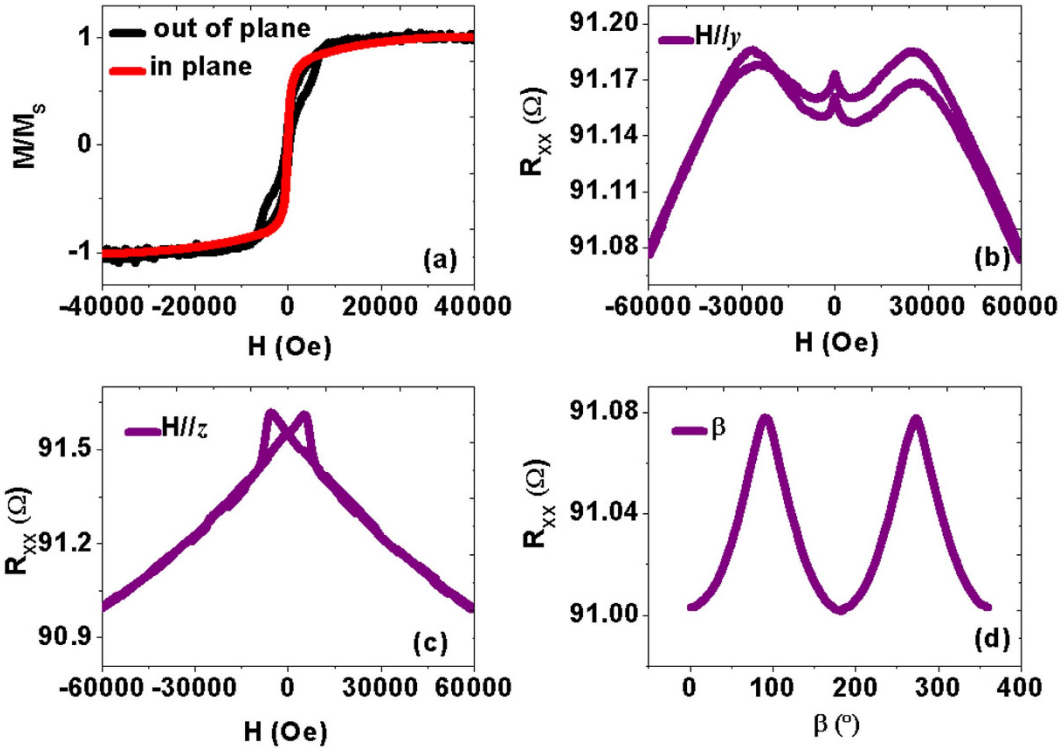

Figure 6. The magnetic and transport properties of MnGa/Pt(1.5)/CoFe/Pt(1.5). (**a**) The normalized out-of-plane and in-plane magnetic hysteresis loops; (**b,c**) The field dependent R_{XX} with **H** along the ***y*** and ***z*** directions respectively; (**d**) β dependence of R_{XX} with a magnetic field of 6 T.

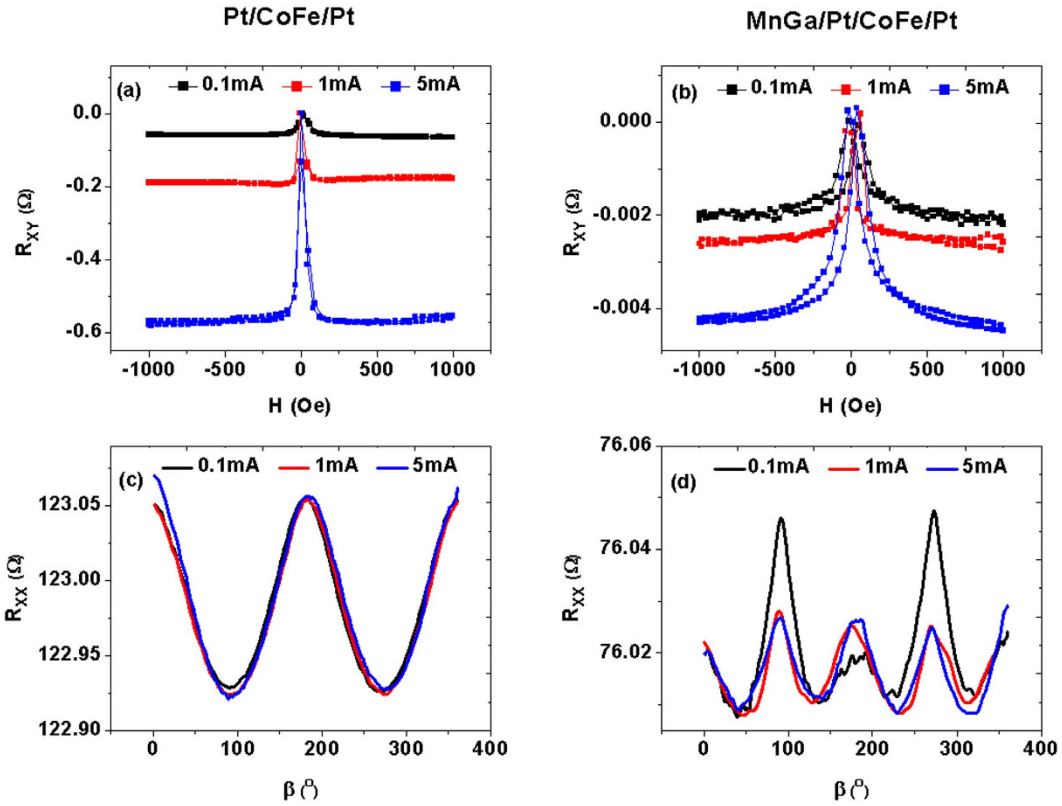

Figure 7. The current dependence of SMR. (**a,b**) Measurements of R_{XY} in Pt/CoFe/Pt and Pt/CoFe/Pt as $\alpha = 135°$ with the current of 0.1, 1 and 5 mA; (**c,d**) β dependence of R_{XX} with a magnetic field of 6 T and the current of 0.1, 1 and 5 mA for the two samples.

from MnGa film as shown in Fig. 3a, while $R_{XX}(\beta)$ are also almost the same with 1 and 5 mA. It is indicated that the SHE may be not the sole origin of the SMR effect, other contributions of NM/FM interfaces, such as, texture induced geometrical size[10] or interfacial Rashba effect[25,26] may be existent, and further study is required to clarify the origin.

In summary, we have investigated the origin of the hybrid MR in Pt/CoFe/Pt, MnGa/Pt and MnGa/Pt/CoFe/Pt multilayers. Both the PHE measured at low field and the angle-dependent MR at high field in Pt/CoFe/Pt revealed the combination of SMR and normal AMR, indicating the large contribution of strong SOC at the interfaces. For MnGa/Pt, the strong interfacial SOC between Pt and PMA MnGa decreased the effective AHE. The MR in MnGa/Pt/CoFe/Pt was not a simple combination of SMR and AMR, but ascribed to the complicated domain wall scattering and strong SOC when Pt was sandwiched between the in-plane magnetized CoFe and PMA MnGa films. Our results provide a way of modulating the spin-related transport effect when strong SOC metals contact with different magnetic anisotropy metals.

Methods

In the experiment, Pt (5)/CoFe (10)/Pt (1.5) (in nanometer) and a reference sample Cu (5)/CoFe (10)/Cu (1.5) were deposited on Si/SiO_2 substrates by dc magnetron sputtering. 20-nm-thick MnGa films were grown on GaAs(001) substrates by molecular beam epitaxy[21], then Pt(t) ($t = 1.5 \sim 5$), Cu(5), Pt(5)/CoFe(10)/Pt(1.5), Pt(1.5)/CoFe(10)/Pt(1.5) and Cu(5)/CoFe(10)/Cu(1.5) were grown on MnGa by dc magnetron sputtering, respectively. The magnetic and transport properties were carried out at room temperature using a superconducting quantum interference device and a physical property measurement system respectively.

References

1. McGuire, T. R. & Potter, R. I. Anisotropic Magnetoresistance in Ferromagnetic 3d Alloys. *IEEE. Trans. Magn*. **MAG-11,** 1018–1038 (1975).
2. Pugh, E. M. & Rostoker, N. Hall Effect in Ferromagnetic Materials. *Rev. Mod. Phys.* **25,** 151 (1953).
3. Fert, A. & Jaoul, O. Left-Right Asymmetry in the Scattering of Electrons by Magnetic Impurities, and a Hall Effect. *Phys. Rev. Lett*. **28,** 303 (1972).
4. Nagaosa, N., Onoda, S., MacDonald, A. H. & Ong, N. P. Anomalous Hall effect. *Rev. Mod. Phys*. **82,** 1539 (2010).
5. Karplus, R. & Luttinger, J. M. Hall Effect in Ferromagnetics. *Phys. Rev*. **95,** 1154 (1954).
6. Huang, S. Y. *et al.* Transport Magnetic Proximity Effects in Platinum. *Phys. Rev. Lett.* **109,** 107204 (2012).
7. Lu, Y. M. *et al.* Pt Magnetic Polarization on $Y_3Fe_5O_{12}$ and Magnetotransport Characteristics. *Phys. Rev. Lett.* **110,** 147207 (2013).
8. Ding, Z. *et al.* Spin Hall magnetoresistance in Pt/Fe_3O_4 thin films at room temperature. *Phys. Rev. B* **90,** 134424 (2014).
9. Li, J. X. *et al.* Pt-enhanced anisotropic magnetoresistance in Pt/Fe bilayers. *Phys. Rev. B* **90,** 214415 (2014).
10. Kobs, A. *et al.* Anisotropic Interface Magnetoresistance in Pt/Co/Pt sandwiches. *Phys. Rev. Lett.* **106,** 217207 (2011).
11. Avci, C. O. *et al.* Unidirectional spin Hall magnetoresistance in ferromagnet/normal metal bilayers. *Nat. Phys*. **11,** 570–575 (2015).
12. Nakayama, H. *et al.* Spin Hall Magnetoresistance Induced by a Nonequilibrium Proximity Effect. *Phys. Rev. Lett.* **110,** 206601 (2013).
13. Chen, Y.-T. *et al.* Theory of spin Hall magnetoresistance. *Phys. Rev. B* **87,** 144411 (2013).
14. Vlietstra, N., Shan, J., Castel, V., van Wees, B. J. & Ben Youssef, J. *et al.* Spin-Hall magnetoresistance in platinum on yttrium iron garnet: Dependence on platinum thickness and in-plane/out-of-plane magnetization. *Phys. Rev. B* **87,** 184421 (2013).
15. Althammer, M. *et al.* Quantitative study of the spin Hall magnetoresistance in ferromagnetic insulator/normal metal hybrids. *Phys. Rev. B* **87,** 224401 (2013).
16. Kimura, T., Otani, Y., Sato, T., Takahashi, S. & Maekawa, S. Room-Temperature Reversible Spin Hall Effect. *Phys. Rev. Lett*. **98,** 156601 (2007).
17. Liu, L. Q., Lee, O. J., Gudmundsen, T. J., Ralph, D. C. & Buhrman, R. A. Current-Induced Switching of Perpendicularly Magnetized Magnetic Layers Using Spin Torque from the Spin Hall Effect. *Phys. Rev. Lett.* **109,** 096602 (2012).
18. Haazen, P. P. J. *et al.* Domain wall depinning governed by the spin Hall effect. *Nature Mater*. **12,** 299–303 (2013).
19. Garello, K. *et al.* Symmetry and magnitude of spin-orbit torques in ferromagnetic heterostructures. *Nature Nanotech*. **8,** 587–973 (2013).
20. Ando, K. *et al.* Electric Manipulation of Spin Relaxation Using the Spin Hall Effect. *Phys. Rev. Lett.* **101,** 036601 (2008).
21. Zhu, L. J. *et al.* Multifunctional $L1_0$-$Mn_{1.5}Ga$ Films with Ultrahigh Coercivity, Giant Perpendicular Magnetocrystalline Anisotropy and Large Magnetic Energy Product. *Adv. Mater.* **24,** 4547 (2012).
22. Zhu, L. J., Pan, D. & Zhao, J. H. Anomalous Hall effect in epitaxial $L1_0$-$Mn_{1.5}Ga$ films with variable chemical ordering. *Phys. Rev. B* **89,** 220406(R) (2014).
23. Levy, P. M. & Zhang, S. Resistivity due to Domain Wall Scattering. *Phys. Rev. Lett*. **79,** 5110 (1997).
24. Viret, M. Samson, Warin, Y. P. Marty, A. Ott, F. Søndergård, E. Klein, O. & Fermon, C. Anisotropy of Domain Wall Resistance. *Phys. Rev. Lett.* **85,** 3962 (2000).
25. Grigoryan, V. L., Guo, W., Bauer, G. E. W. & Xiao, J. Intrinsic magnetoresistance in metal films on ferromagnetic insulators. *Phys. Rev. B* **90,** 161412(R) (2014).
26. Miron, I. M. *et al.* Current-driven spin torque induced by the Rashba effect in a ferromagnetic metal layer. *Nature Mater*. **9,** 230–234 (2010).

Acknowledgements

This work was partially supported by the National Basic Research Program of China (2015CB921502), the National Science Foundation of China (Grant Nos. 61404125, 51371024, 51325101, 51271020).

Author Contributions

K.K.M. and Y.J. conceived and designed the study. K.K.M. and J.X.X. carried out the sample preparation and testing. Y.W., X.G.X. and J.M. gave out the amendments for manuscript. J.H.Z. contributed to the scientific discussions. All authors reviewed the manuscript.

Additional Information

Competing financial interests: The authors declare no competing financial interests.

How to cite this article: Meng, K. *et al.* Hybrid magnetoresistance in Pt-based multilayers: Effect originated from strong interfacial spin-orbit coupling. *Sci. Rep.* **6**, 20522; doi: 10.1038/srep20522 (2016).